Flight Dynamics Modeling and Simulator Design for a New Class of Long-Range Guided Projectiles

Gian Marco Vinco, Spilios Theodoulis, Olivier Sename

Flight Dynamics Modeling and Simulator Design for a New Class of Long-Range Guided Projectiles

Gian Marco Vinco Ph.D. Student, University Grenoble Alpes, CNRS, Grenoble INP, GIPSA-Lab, 38000, Grenoble, France & French-German Research Institute of Saint-Louis, Guidance, Navigation & Control Department, 68300, Saint-Louis, France. gian-marco.vinco@isl.eu

Spilios Theodoulis Senior Research Scientist, French-German Research Institute of Saint-Louis, Guidance, Navigation & Control Department, 68300, Saint-Louis, France. spilios.theodoulis@isl.eu

Olivier Sename Professor, University Grenoble Alpes, CNRS, Grenoble INP, GIPSA-Lab, 38000, Grenoble, France. olivier.sename@grenoble-inp.fr

ABSTRACT

The present research investigates the flight dynamics modeling of a new class of *Long-Range Guided Projectiles* (LRGP), studied at the Institut Franco-Allemand de recherches de Saint-Louis (ISL), and the development of a full 6-DoF nonlinear simulator. The LRGP concept consists of a fin-stabilized projectile, having four rear fins and two horizontal front canards. The canards are mounted in a non-coplanar fashion with respect to the rear fins, in a so-called 'X' configuration. During the simulator design, the equations of motion describing the translational and attitude dynamics & kinematics of the projectile are first illustrated. A major contribution relies on the derivation of a new aerodynamic model based on an extensive regression analysis of the available data. Two full Computational Fluid Dynamics (CFD) campaigns were performed, dealing first with the static characterization of the projectile body, and later more specifically, with the contribution of the canard deflections. For the static characterization of the body, we propose two different regression approaches: a standard *Simple Linear Regression* based on polynomial fitting, and a more advanced *Multivariable Regression*. These approaches are individually investigated, and then cross-compared to assess which one provides with the most reliable results. A second regression analysis is developed in order to model the aerodynamic control contributions given by the canards deflections. The linearity of the canard response is investigated as a function of the Mach variation and of the selection of the regression model complexity. Finally, some trajectory simulations of the overall nonlinear simulator are proposed, as a model design validation.

Keywords: Flight Mechanics Modeling; Regression Analysis; Nonlinear Simulator; Guided Projectiles; Long-Range Projectiles.

1 Introduction

In the last decades, the interest in guided ammunition has grown wider due to the appealing improvements offered in terms of accuracy and operating range. Indeed, classical unguided munitions are highly affected by several factors as launch conditions, wind turbulence and wind gusts, resulting in collateral damages due to the consequent on-target dispersion. One of the main design approaches for the development of guided munitions relies on the employment of aerodynamic control surfaces in the form of nose-mounted canards and/or tail fins. This solution provides with higher control authority for the autopilot design, as well as a continuous-time trajectory correction [1], in comparison to alternative approaches, such as inertial loads or jet thrusters. The airframe stability is generally addressed at the design stage, through the selection between two possible technologies: spin-stabilization or fin-stabilization. The former architecture takes advantage of the aerodynamic forces and moments generated by the high spin rate characterizing the body roll axis, which is transmitted to the projectile at the firing stage.

This particular technology has attracted a relevant interest, leading to the development of several applications in different countries, as for the U.S. ATK's M1156 Precision Guidance Kit (PGK) [2, 3], the French Système à Précision Améliorée par CInémomètre DOppler (SPACIDO) and the U.K. Smart Trajectory Artillery Round (STAR). Relevant research contributions have been carried out also at the Institut Franco-Allemand de recherches de Saint-Louis (ISL), through the studies of Course Correction Fuze (CCF) projectile systems [4–9]. Nevertheless, the spin-stabilized architecture presents also some important drawbacks deriving from the high spin rate characterizing the projectile. Indeed, this effect generates an undesired nonlinear coupling between the normal and the lateral axes dynamics [10], which can represent a non trivial challenge to face during the flight control design. Additionally, spin-stabilized projectiles generally suffer from a limited operating range, depending on the capability of the firing gun and firing conditions.

The enhancement of the range performance, under the avoidance of any modifications of the firing gun, implies the investigation of innovative aerodynamic configurations. A promising solution could be identified in a novel fin-stabilized architecture with a reduced number of control actuators, investigated at ISL, aiming to ameliorate the range capability through a gliding steered flight. Similar approaches can be found in the U.S. M712 Copperhead [11, 12], in the more recent M982 Excalibur [13] and Vulcano. The employment of a non-spinning concept reduces the highly nonlinear dynamics generated by the aerodynamic coupling terms. Thus, the autopilot design can be performed separately for each single axis [14], and the projectile aerodynamics is generally less affected by large and rapid variations of the flight parameters. However, the absence of a high spin rate impacts also negatively on the projectile, requiring specific tail-fins configurations for stability augmentation, and the design of robust autopilots capable to handle the pitch and the roll dynamics.

In this context, the presented study intends to provide a complete description of a new *Long-Range Guided Projectile* (LRGP) concept, studied at ISL, through the design of a full 6-DoF nonlinear simulator, which will be employed for the future autopilot design in the Linear Parameter Varying (LPV) framework. The flight mechanics model of the projectile is first addressed in Section 2, through the presentation of the equations of motion, dealing with the translational and attitude dynamics & kinematics. The main contribution is described in Section 3, namely the aerodynamic characterization of the LRGP concept. Starting from a full Computational Fluid Dynamics (CFD) simulation campaign, we investigate the static aerodynamic properties of the projectile body. To this end, we propose and compare two regression approaches: a *Simple Linear Regression* and a *Multivariable Regression*. A second analysis is later performed in order to model the specific contributions related to the control surfaces deflections. Finally, Section 4 presents the overall nonlinear simulator followed by some preliminary ballistic simulations in the form of design and performance validations.

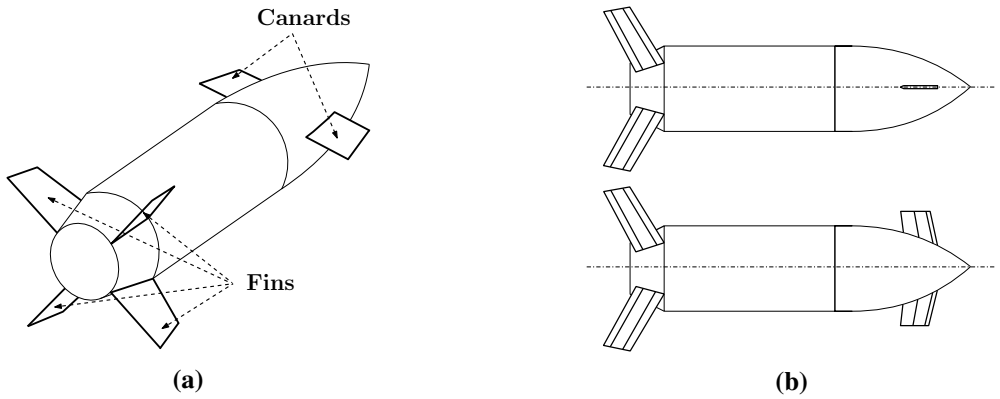

Fig. 1 LRGP concept: (a) aerodynamic surfaces, (b) side and top views.

2 Flight mechanics nonlinear model

The LRGP concept consists of a 155 mm fin-stabilized projectile, mounting a set of four symmetrical rear fins, and two horizontal front canards, in a so-called 'X' configuration, as shown in Fig. 1. This architecture is expected to provide with a lower canard-fin aerodynamic interaction, and a generally reduced angle-of-attack, α, aiming to improve the range performance of the projectile through a gliding trajectory. The gliding phase occurs in subsonic regime conditions.

The 6-DoF nonlinear dynamics governing the LRGP behavior is derived from the standard flight mechanics theory [15, 16], complying with the same notation. The formulation of the equations of motion relies on the definition of two main reference frames. Under the assumption of flat Earth conditions, the Earth frame E, is selected as the inertial reference frame, identified by the triad of base vectors ($\vec{e}_1$, $\vec{e}_2$, $\vec{e}_3$), as in Fig. 2a. A body frame B, attached to the projectile center of gravity (CoG) and coherently rotating with it, is then defined by the base vectors ($\vec{b}_1$, $\vec{b}_2$, $\vec{b}_3$), as in Fig. 2b. In the latter figure, the relative rotations between the airspeed $\vec{v}_B^A$, and the body coordinates is defined through the aerodynamic angle-of-attack and angle-of-sideslip, α and β respectively.

The translational and attitude equations are first derived in tensor form referring to the relative linear and angular motions between the frames B and E, respectively. The dynamic equations in their components form are then expressed with respect to a system of coordinates associated to the main axes of the frame B (see Fig. 2b). Similarly, the kinematic equations are referred to a system of local-level coordinates (North-East-Down, NED) associated to the frame E, but describing the projectile trajectory with respect to a local plane tangent to the Earth surface, independently of its actual geographical longitude and latitude designations.

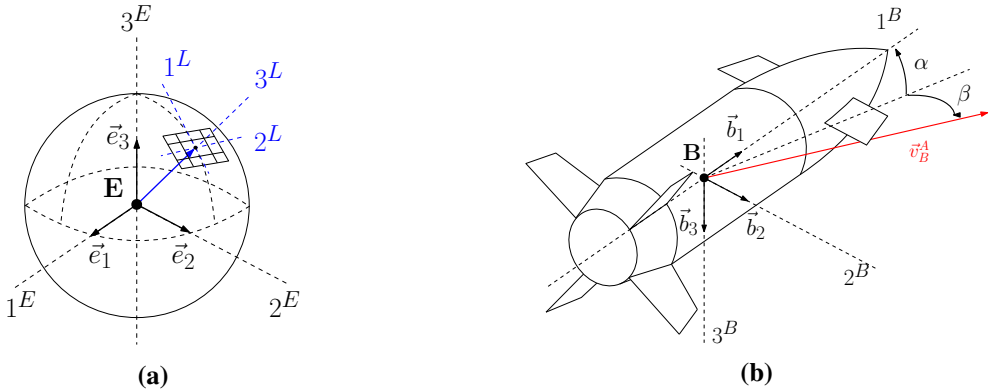

Fig. 2 Main reference frames and coordinate systems: (a) Earth frame, E, and Earth and local coordinates; (b) body frame, B, and body coordinates.

Starting from Newton's and Euler's laws, respectively, the translational and attitude dynamic equations of the projectile are first formulated in tensor form as:

$$mD^{\mathrm{B}}v_{\mathrm{B}}^{\mathrm{E}} + m\Omega^{\mathrm{BE}}v_{\mathrm{B}}^{\mathrm{E}} = f_{\mathrm{aero}} + f_{\mathrm{ctrl}} + f_{\mathrm{grav}}, \tag{1}$$

$$I_{\mathrm{B}}^{\mathrm{B}}D^{\mathrm{B}}\omega^{\mathrm{BE}} + \Omega^{\mathrm{BE}}I_{\mathrm{B}}^{\mathrm{B}}\omega^{\mathrm{BE}} = m_{\mathrm{aero}} + m_{\mathrm{ctrl}}. \tag{2}$$

where D^{B} represents the rotational time derivative operator with respect to the frame B [15].

Equations (1) and (2) are then projected into the body system of coordinates. The resulting sets of state variables for the translational and the attitude dynamic correspond, respectively, to the linear and angular velocities of the frame B with respect to frame E:

$$\left[v_{\mathrm{B}}^{\mathrm{E}}\right]^{\mathrm{B}} = \begin{bmatrix} u_{\mathrm{B}} \\ v_{\mathrm{B}} \\ w_{\mathrm{B}} \end{bmatrix} \quad , \quad \left[\omega^{\mathrm{BE}}\right]^{\mathrm{B}} = \begin{bmatrix} p_{\mathrm{B}} \\ q_{\mathrm{B}} \\ r_{\mathrm{B}} \end{bmatrix}. \tag{3}$$

Moreover, the skew-symmetric form of the angular velocity tensor, ω^{BE}, and the moment of inertia tensor (MoI), are expressed as:

$$\left[\Omega^{\mathrm{BE}}\right]^{\mathrm{B}} = \begin{bmatrix} 0 & -r_{\mathrm{B}} & q_{\mathrm{B}} \\ r_{\mathrm{B}} & 0 & -p_{\mathrm{B}} \\ -q_{\mathrm{B}} & p_{\mathrm{B}} & 0 \end{bmatrix} \quad , \quad \left[I_{\mathrm{B}}^{\mathrm{B}}\right]^{\mathrm{B}} = \begin{bmatrix} I_{\mathrm{x}} & 0 & 0 \\ 0 & I_{\mathrm{y}} & 0 \\ 0 & 0 & I_{\mathrm{z}} \end{bmatrix}. \tag{4}$$

The derivation of the aerodynamic forces (f_{aero}, f_{ctrl}), and moments (m_{aero}, m_{ctrl}), acting on the projectile, is detailed in Section 3. The gravitational contribution, f_{grav}, is simplified to the standard constant acceleration $g = 9.806\,65\,\mathrm{m\,s^{-2}}$, projected from the local to the body system of coordinates, by means of the transformation matrix $[T]^{\mathrm{BL}}$.

Concerning to the kinematics computation, the projectile position, s_{BE}, is expressed with respect to the system of local coordinates (NED). To this end, the linear velocity $v_{\mathrm{B}}^{\mathrm{E}}$, obtained through the translational dynamics in equation (1) in the body coordinates, is first converted to the local coordinates:

$$\left[v_{\mathrm{B}}^{\mathrm{E}}\right]^{\mathrm{L}} = [\bar{T}]^{\mathrm{BL}}\left[v_{\mathrm{B}}^{\mathrm{E}}\right]^{\mathrm{B}} = \begin{bmatrix} u_{\mathrm{L}} \\ v_{\mathrm{L}} \\ w_{\mathrm{L}} \end{bmatrix} \tag{5}$$

and then, the projectile local position can be obtained through time integration, since:

$$\left[\frac{ds_{\mathrm{BE}}}{dt}\right]^{\mathrm{L}} = \left[v_{\mathrm{B}}^{\mathrm{E}}\right]^{\mathrm{L}}. \tag{6}$$

In order to determine the projectile orientation, the rotation tensor approach is preferred [15, 16]. It is based on the formulation of the rotational time derivative of the Direction Cosine Matrix (DCM), $[T]^{\mathrm{BL}}$:

$$\left[\frac{dT}{dt}\right]^{\mathrm{BL}} = \left[\bar{\Omega}^{\mathrm{BE}}\right]^{\mathrm{B}}[T]^{BL}. \tag{7}$$

The resolution of the set of differential equations (7), leads to the evaluation of the Euler angles, (ϕ_{B}, θ_{B}, ψ_{B}), describing the projectile orientation.

3 Aerodynamic model

This section investigates the aerodynamic characterization of the new LRGP concept through the derivation of a suitable model to be included in the proposed nonlinear simulator. In the translational dynamic equation (1), discussed in Section 2, the external forces acting on the projectile have been approximated as the linear superposition of the gravity effect and two additional contributions:

- f_{aero}, which describes the static $(X_{\text{S}}, Y_{\text{S}}, Z_{\text{S}})$, and damping $(Y_{\text{D}}, Z_{\text{D}})$ terms of the full body aerodynamics, assuming zero canard deflections:

$$[f_{\text{aero}}]^{\text{B}} = \begin{bmatrix} X_{\text{B}} \\ Y_{\text{B}} \\ Z_{\text{B}} \end{bmatrix} = \bar{q}S \left\{ \begin{bmatrix} C_{X_{\text{S}}}(M,\alpha,\beta) \\ C_{Y_{\text{S}}}(M,\alpha,\beta) \\ C_{Z_{\text{S}}}(M,\alpha,\beta) \end{bmatrix} + \left(\tfrac{d}{2V}\right) \begin{bmatrix} 0 \\ C_{Y_{\text{D}}}(M,\alpha,\beta)\, r_{\text{B}} \\ C_{Z_{\text{D}}}(M,\alpha,\beta)\, q_{\text{B}} \end{bmatrix} \right\}. \tag{8}$$

- f_{ctrl}, which models the additional control effects $(X_{\text{C}}, Y_{\text{C}}, Z_{\text{C}})$, generated by the local deflection angles of the right and the left canards, δ_{r} and δ_{l}:

$$[f_{\text{ctrl}}]^{\text{B}} = \begin{bmatrix} X_{\text{C}} \\ Y_{\text{C}} \\ Z_{\text{C}} \end{bmatrix} = \bar{q}S \begin{bmatrix} C_{X_{\delta_{\text{eff}}}}(M,\delta_{\text{eff}}) \\ 0 \\ C_{Z_{\delta_q}}(M,\delta_q) \end{bmatrix}. \tag{9}$$

Specifically, in equations (8) and (9), S represents the body reference surface, d the caliber, $\bar{q} = \frac{1}{2}\rho V^2$ the dynamic pressure, and $M = \frac{V}{a}$ the Mach number. These quantities are defined as functions of the air density $\rho = \rho(h)$, and speed of sound $a = a(h)$, depending on the altitude, h. Additionally, V corresponds to the projectile velocity, evaluated as $V = \sqrt{u_{\text{B}}^2 + v_{\text{B}}^2 + w_{\text{B}}^2}$, assuming the air mass to be at rest.

The reader can notice from equation (9) that the control terms are not defined as a function of the individual canard deflection angles, (δ_{r}, δ_{l}), but as a function of a virtual set expressed in terms of the roll and the pitch combined deflections, (δ_p, δ_q). Indeed, a *Control Allocator* has been implemented, in view of the future autopilot design, to target a selected flight strategy, by converting the real control deflections into the more suitable virtual set. The availability of two horizontal front canards, aligned with the intent of improving the range capability of the projectile, suggested the employment of a Bank-To-Turn (BTT) control strategy, leading to the definition of the allocation matrix, T_{CA}:

$$\begin{bmatrix} \delta_p \\ \delta_q \end{bmatrix} = \begin{bmatrix} -\frac{1}{2} & +\frac{1}{2} \\ +\frac{1}{2} & +\frac{1}{2} \end{bmatrix} \begin{bmatrix} \delta_{\text{r}} \\ \delta_{\text{l}} \end{bmatrix} = [T_{\text{CA}}] \begin{bmatrix} \delta_{\text{r}} \\ \delta_{\text{l}} \end{bmatrix}. \tag{10}$$

Additionally, the longitudinal control term, $C_{X_{\delta_{\text{eff}}}}$, is affected by the combined nonlinear contributions of roll and pitch, defined as $\delta_{\text{eff}} = \sqrt{\delta_p^2 + \delta_q^2}$.

Similarly, the aerodynamic moments in equation (2) are also approximated as the sum of a static and damping full body term, m_{aero}, and a control contribution, m_{ctrl}:

$$[m_{\text{aero}}]^{\text{B}} = \begin{bmatrix} L_{\text{B}} \\ M_{\text{B}} \\ N_{\text{B}} \end{bmatrix} = \bar{q}Sd \left\{ \begin{bmatrix} C_{l_{\text{S}}}(M,\alpha,\beta) \\ C_{m_{\text{S}}}(M,\alpha,\beta) \\ C_{n_{\text{S}}}(M,\alpha,\beta) \end{bmatrix} + \left(\tfrac{d}{2V}\right) \begin{bmatrix} 0 \\ C_{m_{\text{D}}}(M,\alpha,\beta)\, q_{\text{B}} \\ C_{n_{\text{D}}}(M,\alpha,\beta)\, r_{\text{B}} \end{bmatrix} \right\}, \tag{11}$$

$$[m_{\text{ctrl}}]^{\text{B}} = \begin{bmatrix} L_{\text{C}} \\ M_{\text{C}} \\ N_{\text{C}} \end{bmatrix} = \bar{q}Sd \begin{bmatrix} C_{l_{\delta_p}}(M,\delta_p) \\ C_{m_{\delta_q}}(M,\delta_q) \\ 0 \end{bmatrix}. \tag{12}$$

The global coefficients defining the body and control terms of the aerodynamic forces (C_{X_S}, C_{Y_S}, C_{Z_S}, $C_{X_{\delta_{\text{eff}}}}$, $C_{Z_{\delta_q}}$), and moments (C_{l_S}, C_{m_S}, C_{n_S}, $C_{l_{\delta_p}}$, $C_{m_{\delta_q}}$), have been modeled through an extensive regression analysis based on two datasets of Computational Fluid Dynamics (CFD) simulations.

- The first simulation campaign, analyzed in Section 3.1, is intended to characterize the static aerodynamics of the full projectile body, by measuring the global aerodynamic forces and moments (X_B, Y_B, Z_B, l_B, m_B, n_B). The non-dimensional coefficients were obtained through the normalization of the measurements with respect to the projectile dimensions. The data were first acquired as a function of the Mach number in the subsonic regime, $M \in [M_{\min}, \dots, M_{\max}]$, the aerodynamic roll angle, $\phi' \in [0^\circ, \dots, 90^\circ]$, and the total angle-of-attack, $\alpha' \in \left[\alpha'_{\min}, \dots, \alpha'_{\max}\right]$, more suitable for the CFD environment and coherent with the actual wind tunnel test procedure. Thus once M, and ϕ', were fixed, the coefficients were investigated across the variation of α'. For modeling coherence, the coefficients have been later converted to the Cartesian incidence angles, (α, β):

$$\alpha = \arctan\left(\tan\alpha' \cos\phi'\right) \quad , \quad \beta = \arcsin\left(\sin\alpha' \sin\phi'\right). \tag{13}$$

- The second simulation campaign is used in Section 3.2, and it is focused on the aerodynamic contributions, (X_C, Z_C, L_C, M_C), generated by the canard local deflections, δ_r and δ_l. During the analysis, the angles ϕ' and α' were set to zero, in order to avoid any undesired body interaction. In particular, the data were acquired only with respect to the right canard through the investigation of the same M range, and across the local deflection range, $\delta_r \in [0^\circ, \dots, \delta_{r,\max}]$. The aerodynamic coefficients related to the left canard could be easily obtained by means of symmetrical considerations. The modeling procedure that converts the real canard deflection coefficients, ($C_{X_{\delta_r}}$, $C_{Z_{\delta_r}}$, $C_{l_{\delta_r}}$, $C_{m_{\delta_r}}$), measured by the CFD simulations, into the corresponding virtual counterparts, ($C_{X_{\delta_{\text{eff}}}}$, $C_{Z_{\delta_q}}$, $C_{l_{\delta_p}}$, $C_{m_{\delta_q}}$), is based on equations (10) and later discussed in detail.

3.1 Body aerodynamic contribution

In order to properly model the static contribution of the projectile, the CFD dataset related to the first simulation campaign has been investigated by means of two different regression approaches: a standard *Simple Linear Regression* and a more sophisticated *Multivariable Regression*.

3.1.1 Simple Linear Regression

The first approach relies on the analysis of a reduced set of CFD data, and specifically, on the measurements related to the extreme configurations where $\phi' = 0^\circ$ or $\phi' = 90^\circ$. According to equation (13), in the former case the measured coefficients result to be inspected across the variation of α, without any contribution deriving from β. The latter case addresses the completely opposite scenario, since the aerodynamics of the projectile strictly depends only on the variation of β. These assumptions allowed the employment of a standard polynomial regression with least-squares optimization. Several polynomial models of increasing order have been investigated for each of the aerodynamic coefficients, aiming to find the best compromise between regression accuracy and model complexity.

Depending on the selected configuration, the estimated regression parameters correspond either to the set of α coefficient derivatives, or to the β ones. The analysis has been repeated for all the considered Mach conditions, $M \in [M_{\min}, \dots, M_{\max}]$. The accuracy is assessed by means of the standard statistical indexes: Sum of Squared Errors (SSE), Root Mean Squared Error (RMSE), and Coefficient of Determination (R^2). The R^2 results obtained during the regression of the α derivatives are displayed in Fig. 3[1]. In particular, for each of the aerodynamic coefficients, only the most relevant derivatives have been included in the final model, meaning that either the α or β set of derivatives have been considered, to reduce the overall mathematical complexity.

[1]The Mach number values have been rescaled for confidentiality reasons.

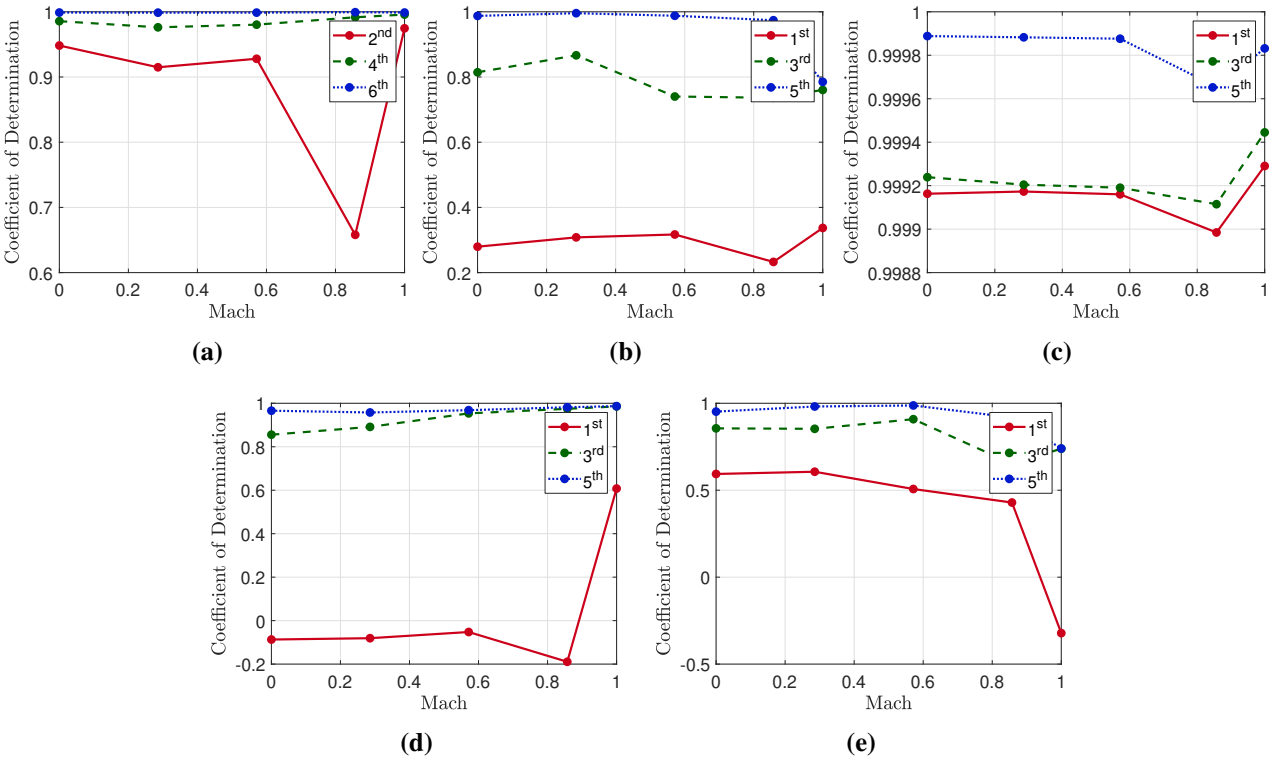

Fig. 3 R^2 results: (a) longitudinal force, (b) lateral force, (c) vertical force, (d) pitching moment, (e) yawing moment.

Based on the statistical results, the following *Simple Linear Regression* model is proposed:

$$\begin{aligned}
C_{X_S}(M,\alpha) &= C_{X_{\alpha 0}}(M) + C_{X_{\alpha 2}}(M)\sin^2\alpha + C_{X_{\alpha 4}}(M)\sin^4\alpha,\\
C_{Y_S}(M,\beta) &= C_{Y_{\beta 1}}(M)\sin\beta,\\
C_{Z_S}(M,\alpha) &= C_{Z_{\alpha 1}}(M)\sin\alpha,\\
C_{m_S}(M,\alpha) &= C_{m_{\alpha 1}}(M)\sin\alpha + C_{m_{\alpha 3}}(M)\sin^3\alpha + C_{m_{\alpha 5}}(M)\sin^5\alpha,\\
C_{n_S}(M,\beta) &= C_{n_{\beta 1}}(M)\sin\beta.
\end{aligned} \tag{14}$$

It is important to notice that the rolling moment coefficient, C_{l_S}, has not been included in the proposed model, since its contribution is negligible in comparison to the other coefficients.

3.1.2 Multivariable Regression

The second approach relies on the analysis of all the available CFD data, addressing also the coupling effects generated by the simultaneous variation of the angles α and β. Having to deal with several variables, sets of multivariable models have been selected for the data regression. In particular, each of the coefficients has been investigated through the comparison of three different models:

- **Test Function**: selected among a large set of trial models in the form of standard multivariable polynomials with increasing order, in reason of the higher capability to fit the CFD dataset.
- **Formula Function**: derived from theoretical flight mechanics considerations [17]. It consists of the theoretical formulation of the selected aerodynamic force/moment, expressed in its components form with respect to the body coordinates system.
- **Independent Function**: intended to model the impact of the angles variation by means of independent regression coefficients, each as a derivative of either α or β; thus, no bilinear terms are included in the model.

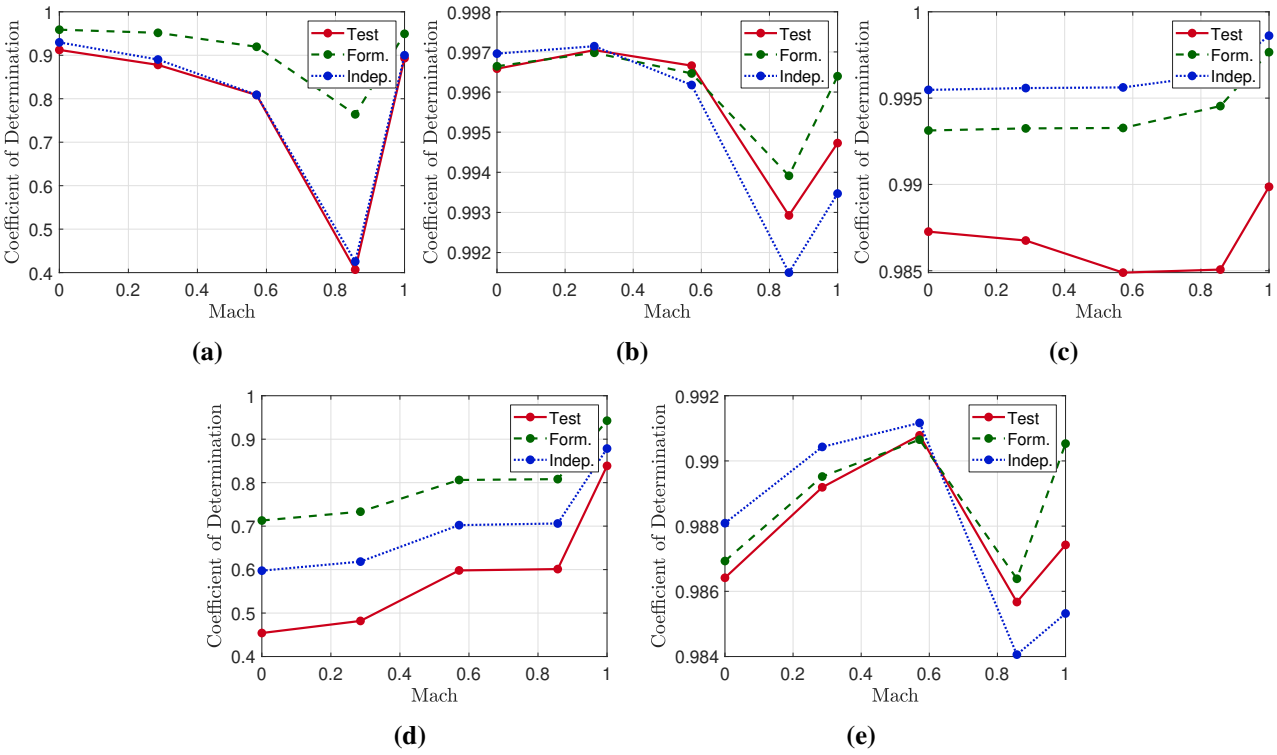

Fig. 4 R^2 results: (a) longitudinal force, (b) lateral force, (c) vertical force, (d) pitching moment, (e) yawing moment.

As for the *Simple Linear Regression*, the accuracy of the investigated models is assessed by means of the statistical indexes (SSE, RMSE, R^2). The complete set of R^2 results is presented in Fig. 4[2].

As a general trend, the results show how the set of Formula Functions proposed below provides the most reliable description of the projectile aerodynamics, based on the full CFD dataset. The pitching moment revealed to be the most difficult coefficient to be properly modeled because of the highly nonlinear influence deriving from the β variation. The final model obtained through the *Multivariable Regression* analysis corresponds to:

$$\begin{aligned}
C_{X_S}(M,\alpha,\beta) &= C_{X_0}(M) + C_{X_2}(M)\cos\alpha\cos\beta + C_{X_4}(M)\cos^2\alpha\cos^2\beta,\\
C_{Y_S}(M,\alpha,\beta) &= C_{Y_1}(M)\sin\beta + C_{Y_2}(M)\sin\alpha,\\
C_{Z_S}(M,\alpha,\beta) &= C_{Z_2}(M)\sin\alpha\cos\beta,\\
C_{m_S}(M,\alpha,\beta) &= C_{m_2}(M)\sin\alpha\cos\beta + C_{m_4}(M)\sin\alpha\cos\alpha\cos^2\beta,\\
C_{n_S}(M,\alpha,\beta) &= C_{n_1}(M)\sin\beta + C_{n_2}(M)\sin\alpha.
\end{aligned} \tag{15}$$

Once again, the reader can notice how the rolling moment coefficient, C_{l_S}, has not been included in the overall model for the same reasons previously discussed.

3.1.3 Regression approaches comparison

The analysis of the CFD data resulted in two different aerodynamic models: the *Simple Linear* (equation (14)) based on the reduced set of data, and the *Multivariable* (equation (15)) relying on the full dataset. Aiming to point out the limitations of the former approach, we developed a cross-comparison between the two models. However, since the models have been derived from different datasets, the previously obtained statistical results, (SSE, RMSE, R^2), couldn't be directly compared.

[2]The Mach number values have been rescaled for confidentiality reasons.

As a consequence, an additional interpolation error analysis has been carried out. The value of each aerodynamic coefficient is interpolated first directly on the CFD surfaces, as a ground truth reference. Then, the same interpolation is performed on the modeled surfaces obtained through the two regression approaches. The process is repeated across the full range of M, ϕ' and α' investigated during the CFD simulation campaigns.

The interpolation error, e, is evaluated as the difference between the results provided by the CFD coefficient interpolations, C_{CFD}, and the selected model ones, C. Furthermore, the mean value of the error is computed along the α' variation, by selecting iteratively a specific pair of (M, ϕ'). These settings allowed us to observe the variation of the interpolation error, as a function of the increasing roll configuration, and consequently of the different (α, β) combinations, as well as of the Mach number. The mean error is normalized by the corresponding CFD mean value, as follow:

$$\bar{e}_{\text{norm}}\left(M, \phi', \alpha'\right) = \frac{\bar{e}(M, \phi', \alpha')}{\bar{C}_{\text{CFD}}(M, \phi', \alpha')} \tag{16}$$

and we define

$$\bar{e}\left(M, \phi', \alpha'\right) = \frac{\sum_{i=1}^{n} \left(C_i(M, \phi', \alpha') - C_{\text{CFD},i}(M, \phi', \alpha')\right)}{n}, \tag{17}$$

$$\bar{C}_{\text{CFD}}\left(M, \phi', \alpha'\right) = \frac{\sum_{i=1}^{n} C_{\text{CFD},i}(M, \phi', \alpha')}{n}, \tag{18}$$

where n is the dimension of the investigated α' range.

The results displayed in Fig. 5[3] give an example of the variation of the interpolation error related to the pitching moment coefficient, as a function of the increasing roll configuration.

As expected, for an initial configuration of $\phi' = 0°$ (example in Fig. 5a), the *Simple Linear Regression* is in general capable to better describe the aerodynamics of the projectile, which depends only on α. Nevertheless, as soon as the roll is increased (example in Figs. 5b-5c), the *Simple Linear Regression* method does not compare any longer with the *Multivariable Regression*.

The same observations are confirmed in Fig. 6[4] from a graphical perspective. Indeed, the comparison between the two modeled interpolation surfaces, related to the pitching moment, shows how the *Multivariable* model manages to fit the available CFD measurements with higher accuracy than the *Simple Linear* one.

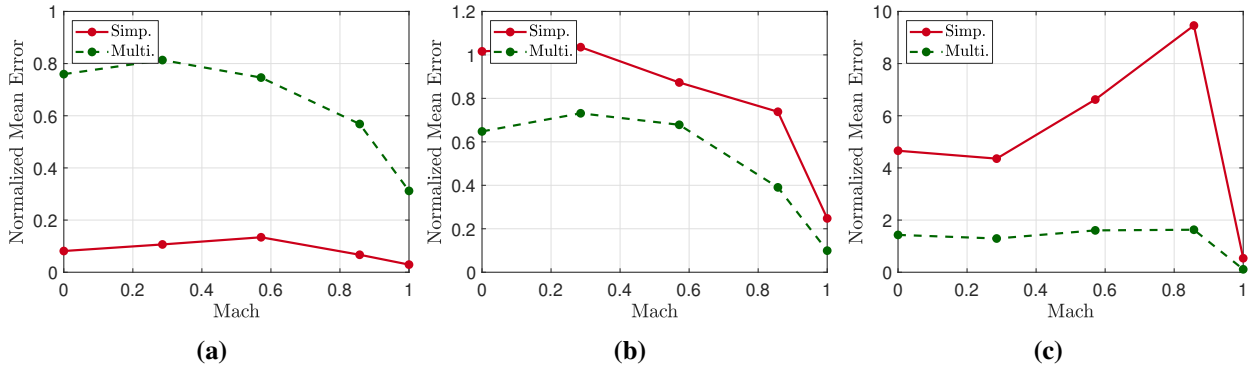

Fig. 5 Pitching moment models: (a) interpolation error at $\phi' = 0°$; (b)-(c) interpolation error for increasing values of ϕ'.

[3]The Mach number values have been rescaled for confidentiality reasons.

[4]The aerodynamic angles and the coefficient values have been rescaled for confidentiality reasons.

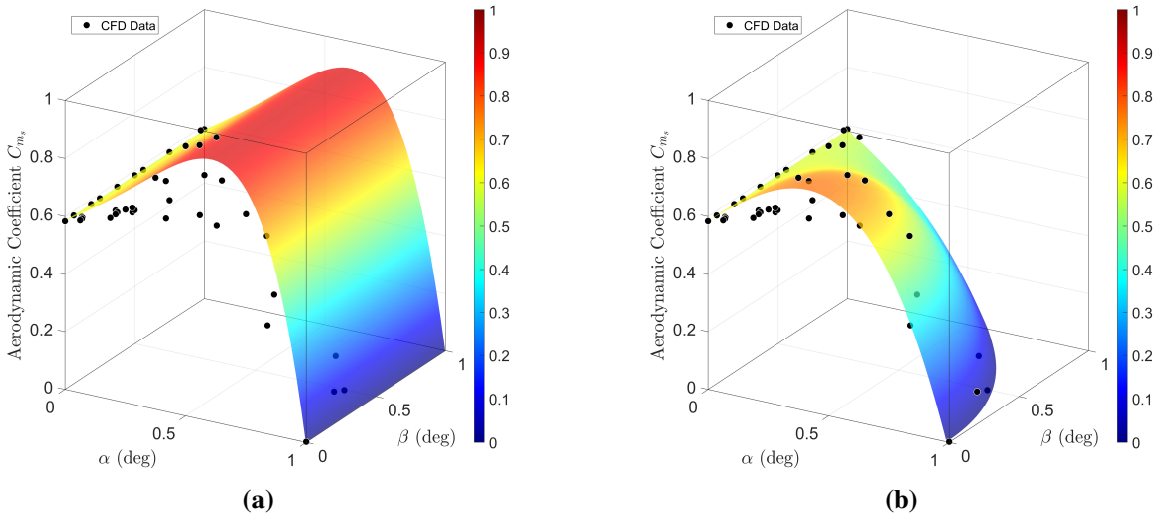

Fig. 6 Pitching moment models: (a) *Simple Linear* interpolation surface; (b) *Multi-variable* interpolation surface.

3.2 Canards aerodynamic contributions

The second campaign of CFD simulations focused on the characterization of the right canard local deflection, δ_r. Dealing only with one angle variation, the standard polynomial regression approach is enough accurate to provide with reliable models for $C_{X_{\delta_\mathrm{r}}}$, $C_{Z_{\delta_\mathrm{r}}}$, $C_{l_{\delta_\mathrm{r}}}$ and $C_{m_{\delta_\mathrm{r}}}$. The corresponding left counterparts, associated to δ_l, were inferred from symmetrical considerations. The overall control contributions, generated by the canard deflections, could be computed by superposition, assuming the aerodynamic response of the canards to be in a linear domain:

$$C_{X_\delta}(M,\delta) = C_{X_{\delta_\mathrm{r}}}(M,\delta_\mathrm{r}) + C_{X_{\delta_\mathrm{l}}}(M,\delta_\mathrm{l}), \tag{19}$$

$$C_{Z_\delta}(M,\delta) = C_{Z_{\delta_\mathrm{r}}}(M,\delta_\mathrm{r}) + C_{Z_{\delta_\mathrm{l}}}(M,\delta_\mathrm{l}), \tag{20}$$

$$C_{l_\delta}(M,\delta) = C_{l_{\delta_\mathrm{r}}}(M,\delta_\mathrm{r}) + C_{l_{\delta_\mathrm{l}}}(M,\delta_\mathrm{l}), \tag{21}$$

$$C_{m_\delta}(M,\delta) = C_{m_{\delta_\mathrm{r}}}(M,\delta_\mathrm{r}) + C_{m_{\delta_\mathrm{l}}}(M,\delta_\mathrm{l}), \tag{22}$$

where the lateral and the yaw control coefficients, (C_{Y_δ}, C_{n_δ}), are ignored due to the absence of control authority on the yaw plane.

However, as previously discussed, the control allocator embedded in the simulator converts the individual deflections of the canards into a combined set of virtual contributions, δ_p and δ_q (equation (10)). Coherently, the aerodynamic models have to address the virtual set of coefficients, ($C_{X_{\delta_\mathrm{eff}}}$, $C_{Z_{\delta_q}}$, $C_{l_{\delta_p}}$, $C_{m_{\delta_q}}$ in Fig. 7), instead of the global contributions in equations (19-22). Nevertheless, no CFD data related to the virtual deflections were available.

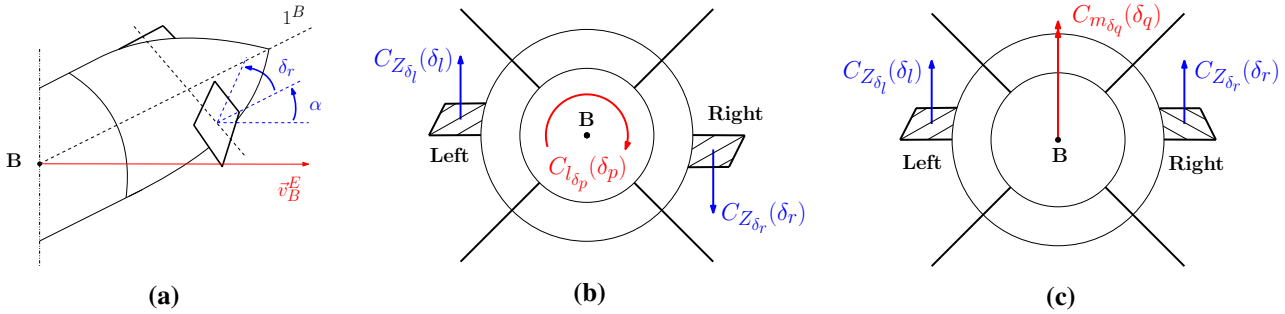

Fig. 7 Deflections: (a) individual; (b) virtual roll; (c) virtual pitch.

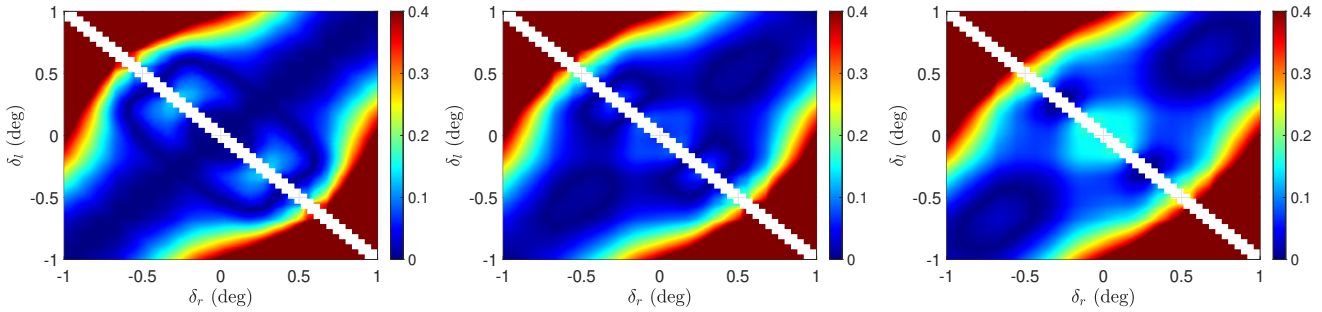

(a) **(b)** **(c)**

Fig. 8 Pitching moment: e_l deriving from the (a) interpolation on the CFD surface; (b) interpolation on a 5th order model; (c) interpolation on a 3rd order model.

A possible solution could be found in equation (10), through the definition of the virtual deflections. Indeed, according to the linearity assumptions, the superposition results described in equations (19-22) could be approximated as the direct interpolation of the corresponding virtual coefficients on the available regression surfaces. By referring to the vertical force coefficient as example, a linear aerodynamic response can be assumed as:

$$\begin{aligned} C_{Z_\delta}(M,\delta) &= C_{Z_{\delta_r}}(M,\delta_r) + C_{Z_{\delta_l}}(M,\delta_l) \\ &\simeq 2\, C_{Z_{\delta_q}}(M,\delta_q) = 2\, C_{Z_{\delta_q}}\left(M, \frac{\delta_r+\delta_l}{2}\right). \end{aligned} \tag{23}$$

In order to verify in which deflection range the previous relation holds, a linearity error, e_l, is evaluated as the difference between the global coefficients, (C_{X_δ}, C_{Z_δ}, C_{l_δ}, C_{m_δ}) and the virtual ones ($C_{X_{\delta_{\text{eff}}}}$, $C_{Z_{\delta_q}}$, $C_{l_{\delta_p}}$, $C_{m_{\delta_q}}$), normalized by the corresponding CFD values. The analysis has been extended to the entire deflection range and Mach values investigated during the CFD simulations. In particular, Fig. 8[5]shows an example related to how the selection of the regression model complexity affects the linearity error of the pitching moment coefficient, for a fixed Mach number.

The deflection range corresponding to a linearity error $e_l \leq 10\%$ is wider when the coefficients are interpolated directly on the CFD surfaces (Fig. 8a), but tends to decrease when interpolated on the regression surfaces due to the limited accuracy, as the order of the polynomial models decreases (Figs. 8b-8c). Similar results can be observed in terms of Mach contributions. Indeed, Fig. 9[5] shows how the same deflection range is highly affected by the increase of the Mach value, when a 3rd order polynomial model is employed. As a global result, we could assess that the linear approximations formulated in equation (23), provide with reliable modeling properties for canard deflections $\delta_r, \delta_l \in [-25°, 25°]$.

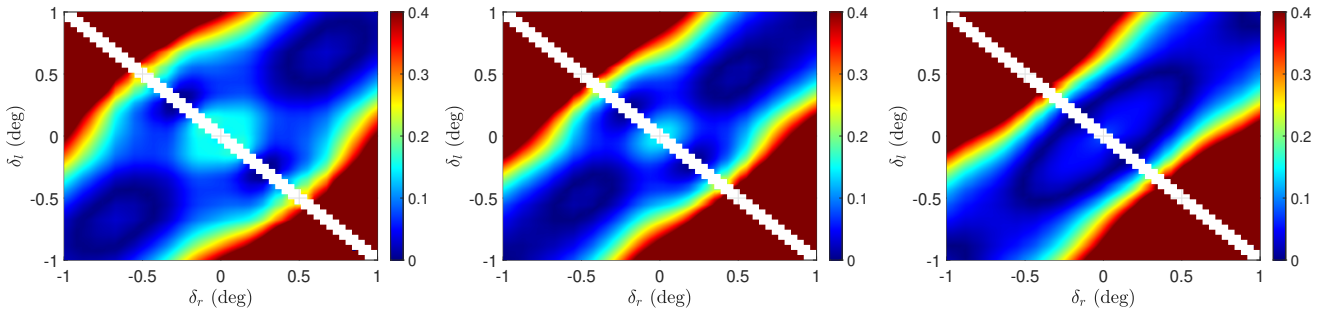

(a) **(b)** **(c)**

Fig. 9 Pitching moment: e_l related to increasing values of the Mach number.

[5]The deflection angle values have been rescaled for confidentiality reasons.

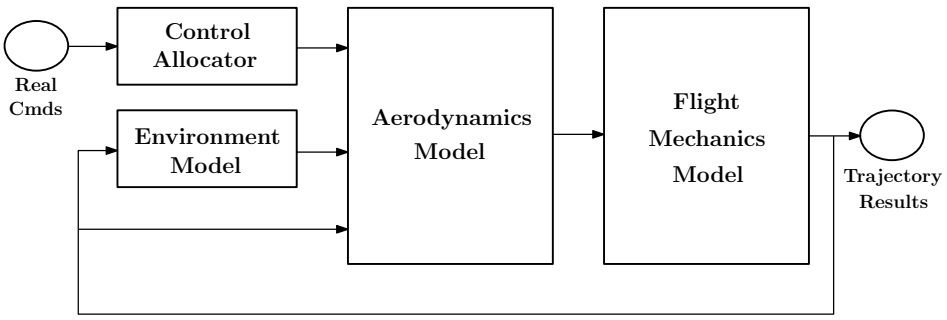

Fig. 10 Overview of the airframe nonlinear simulator scheme.

4 The ballistic simulator

After the derivation of the projectile flight mechanics (equations (1-2)), discussed in Section 2, the allocation matrix T_{CA} (equation (10)), and the investigation of the aerodynamic model, proposed in Section 3, we can finally present the overall design of the 6-DoF nonlinear simulator for the LRGP concept. The airframe block scheme shown in Fig. 10, provides an overview about the architecture of the simulator, which has been realized by means of the System Modeling Ammunition Research Toolbox (SMART), developed at ISL. More in details, it additionally includes:

- **Environment Model**: where the atmosphere is modeled following the International Standard Atmosphere (ISA) 1975, ISO 2533 [18]. According to the flat Earth approximations, the gravity is simplified to the standard constant acceleration along the normal axis direction. The wind contributions are also modeled, including constant horizontal wind, wind gusts and turbulence.
- **Aerodynamics Model**: based on the results presented in Section 3, concerning the static and control aerodynamic contributions, the following full model is implemented:

$$
\begin{aligned}
C_X(M,\alpha,\beta,\delta_{\mathrm{eff}}) &= C_{X_0}(M) + C_{X_2}(M)\cos\alpha\cos\beta + C_{X_4}(M)\cos^2\alpha\cos^2\beta + \\
&\quad + C_{X_{\delta 0}}(M) + C_{X_{\delta 2}}(M)\sin^2\delta_{\mathrm{eff}}, \\
C_Y(M,\alpha,\beta) &= C_{Y_1}(M)\sin\beta + C_{Y_2}(M)\sin\alpha, \\
C_Z\big(M,\alpha,\beta,\delta_q\big) &= C_{Z_2}(M)\sin\alpha\cos\beta + C_{Z_{\delta 1}}(M)\sin\delta_q + C_{Z_{\delta 3}}(M)\sin^3\delta_q, \\
C_l(M,\alpha,\beta,\delta_p) &= C_{l_{\delta 1}}(M)\sin\delta_p + C_{l_{\delta 3}}(M)\sin^3\delta_p, \\
C_m\big(M,\alpha,\beta,\delta_q\big) &= C_{m_2}(M)\sin\alpha\cos\beta + C_{m_4}(M)\sin\alpha\cos\alpha\cos^2\beta + \\
&\quad + C_{m_{\delta 1}}(M)\sin\delta_q + C_{m_{\delta 3}}(M)\sin^3\delta_q, \\
C_n(M,\alpha,\beta) &= C_{n_1}(M)\sin\beta + C_{n_2}(M)\sin\alpha.
\end{aligned}
\tag{24}
$$

Aiming to verify the reliability of the simulator in terms of aerodynamics and flight mechanics modeling coherence, some ballistic simulations have been performed, neglecting any control deflections and wind disturbances. To this end, Fig. 11 shows the trajectories related to some flight tests having the same launch conditions, but with the progressive inclusion of the aerodynamic contributions. In particular, 'G' indicates a trajectory affected only by the gravity effect, 'D' assumes also the drag contribution, 'L' the lift force, and finally, a 5-DoF simulation addresses all the aerodynamic forces and moments except for the pitching moment, since it is expected to generate instability in the projectile dynamics.

More in details, Fig. 12 displays the curve related to the pitching moment generated during the 5-DoF simulation. It is possible to observe how, for positive values of α, and in a specific range of Mach number, the pitching moment assumes positive values as well, leading to an unstable trajectory. Thus, it is not possible to provide a clean open loop simulation addressing also this contribution. Nevertheless, an important drawback deriving from the previous assumption, consists of the projectile elevation angle, θ_{B}, imposed as initial condition, which remains constant during the entire trajectory.

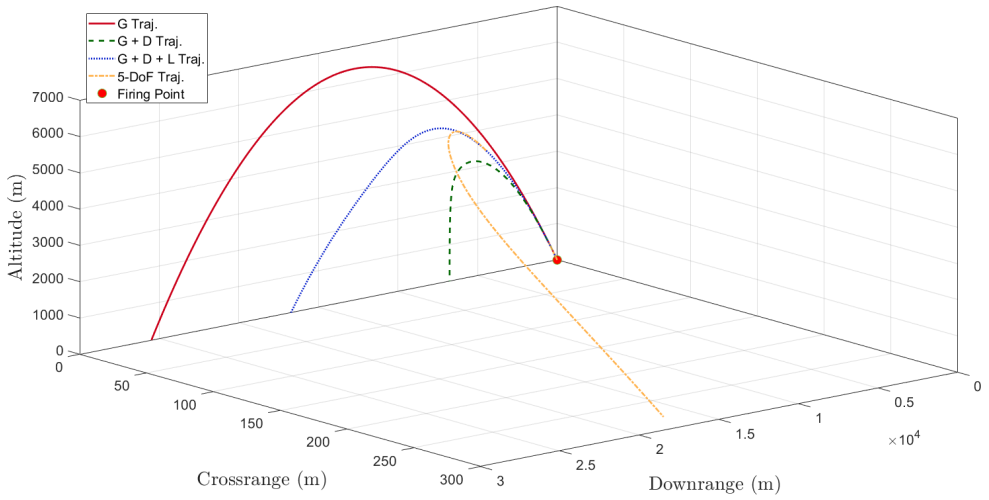

Fig. 11 Simulated trajectory results.

Due to the constant attitude of the projectile, α tends to increase as a function of the trajectory shape, reaching very high values, (up to 100°), during the gliding and the terminal phases of the flight.

In this context, the main problem arises when α reaches values that exceed the CFD dataset investigated during the aerodynamic models regressions, leading to the extrapolation of the aerodynamic coefficients. As a consequence, the simulator is no longer capable to provide a reliable characterization of the projectile aerodynamic, and the resulting trajectories become meaningless. To address this issue, a constant stabilizing pitching moment has been imposed as initial condition for the presented simulations, trying to force the projectile orientation to follow the trajectory, thus ensuring to maintain the variation of α in a reasonable range.

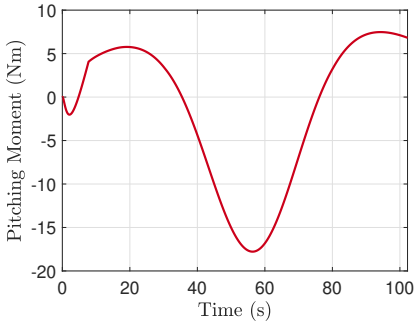

Fig. 12 5-DoF simulation: pitching moment curve.

However, this expedient does not question the relevance of the results in terms of design validation, especially keeping in mind that the projectile is intended to be equipped with a pitch controller that will correct the unstable behavior observed in the simulations.

5 Conclusion and future works

In this article, a nonlinear airframe model describing the dynamics of the new 155 mm fin-stabilized LRGP concept is investigated. The equations of motion are formulated from the standard flight mechanics literature. A reliable aerodynamic model is successfully derived through the comparison between two different regression approaches, from a full set of CFD data. A statistical and a graphical interpretations of the interpolation results prove the higher fidelity of the *Multivariable* approach over the more standard *Simple Linear Regression*. A second regression analysis on aerodynamic canard contributions, ensures an interpolation error e_l lower than 10% inside a linear deflections range $\delta_r, \delta_l \in [-25°, 25°]$. Finally, the overall nonlinear model is implemented and tested in simulation showing an unstable behavior generated by a destabilizing pitching moment, as expected from the analysis of the CFD measurements.

In terms of future efforts, the presented nonlinear model is intended to be used to develop a robust control system, in view of the design of a pitch and roll channels autopilot. A BTT flight control strategy is expected to be aligned with the aim of enhancing the range capability of the ammunition. Possible model improvements will be also considered, concerning the extension of the equations of motion to the elliptical Earth assumption, or the employment of advanced sensor and actuator models.

Acknowledgments

The authors would like to thank Dr. Michel Libsig and Dr. Simon Bagy from the Institut Franco-Allemand de recherches de Saint-Louis (ISL), for the contribution they made to this research by providing the projectile aerodynamic data necessary for the analysis.

References

[1] Kevin A. Wise and David J. B. Roy. Agile missile dynamics and control. *Journal of Guidance, Control, and Dynamics*, 21(3):441–449, May 1998. DOI: 10.2514/2.4256.

[2] Doug Storsved. PGK and the impact of affordable precision on the fires mission. In *Proceedings of the 43rd Annual Guns & Missiles Symposium*, pages 21–24, New Orleans, LA, USA, April 2008.

[3] Thomas Pettersson, Richard Buretta, and David Cook. Aerodynamics and flight stability for a course corrected artillery round. In *Proceedings of the 23rd International Symposium on Ballistics*, Tarragona, Spain, April 2007.

[4] Spilios Theodoulis, Yannick Morel, and Philippe Wernert. Modelling and stability analysis of the 155 mm spin-stabilised projectile equipped with steering fins. *International Journal of Modelling, Identification and Control*, 14(3):189–204, September 2011. DOI: 10.1504/IJMIC.2011.042655.

[5] Spilios Theodoulis and Philippe Wernert. Flight control for a class of 155 mm spin-stabilized projectiles with course correction fuse (CCF). In *Proceedings of the 2011 AIAA Guidance, Navigation, and Control Conference*, page 6247, Portland, OR, USA, August 2011.

[6] Spilios Theodoulis, Florian Sève, and Philippe Wernert. Robust gain-scheduled autopilot design for spin-stabilized projectiles with a course-correction fuze. *Aerospace Science and Technology*, 42:477–489, April 2015. DOI: 10.1016/j.ast.2014.12.027.

[7] Florian Seve, Spilios Theodoulis, Philippe Wernert, Michel Zasadzinski, and Mohamed Boutayeb. Flight dynamics modeling of dual-spin guided projectiles. *IEEE Transactions on Aerospace and Electronic Systems*, 53(4):1625–1641, February 2017. DOI: 10.1109/TAES.2017.2667820.

[8] Sovanna Thai, Spilios Theodoulis, Clément Roos, and Jean-Marc Biannic. Robust design for the roll-channel autopilot of a canard-guided dual-spin projectile. *IFAC-PapersOnLine*, 52(12):232–237, August 2019. DOI: 10.1016/j.ifacol.2019.11.248.

[9] Sovanna Thai, Spilios Theodoulis, Clément Roos, Jean-Marc Biannic, and Michael Proff. Gain-scheduled autopilot design with anti-windup compensator for a dual-spin canard-guided projectile. In *Proceedings of the 2020 IEEE Conference on Control Technology and Applications (CCTA)*, pages 156–161, Montreal, QC, Canada, August 2020.

[10] K.H. Lloyd and D.P. Brown. Instability of spinning projectiles during terminal guidance. *Journal of Guidance and Control*, 2(1):65–70, January 1979. DOI: 10.2514/3.55833.

[11] Phillip H. Morrison and David S. Amberntson. Guidance and control of a cannon-launched guided projectile. *Journal of Spacecraft and Rockets*, 14(6):328–334, June 1977. DOI: 10.2514/3.57205.

[12] Robert A. Nulk, Harold L. Pastricky, and Phillip A. Morrison. Copperhead semiactive laser guidance system development. *Journal of Guidance and Control*, 2(5):374–381, September 1979. DOI: 10.2514/3.55892.

[13] Lawrence L. Wells. The projectile GRAM SAASM for ERGM and excalibur. In *Proceedings of the IEEE 2000 Position Location and Navigation Symposium*, pages 106–111, San Diego, CA, USA, March 2000.

[14] John H. Blakelock. *Automatic control of aircraft and missiles*. John Wiley & Sons, 1991.

[15] Peter H. Zipfel. *Modeling and Simulation of Aerospace Vehicle Dynamics*. American Institute of Aeronautics and Astronautics, Inc., 3rd edition, June 2014.

[16] Peter H. Zipfel. Aerodynamic symmetry of aircraft and guided missiles. *Journal of Aircraft*, 13(7):470–475, July 1976. DOI: 10.2514/3.44536.

[17] Robert McCoy. *Modern exterior ballistics: The launch and flight dynamics of symmetric projectiles*. Schiffer Pub., 1999.

[18] International Organization for Standardization. Standard atmosphere. Standard, May 1975. ISO 2533:1975.